Deep-Sea Research II 122 (2015) 41–51

Contents lists available at ScienceDirect

Deep-Sea Research II

journal homepage: www.elsevier.com/locate/dsr2

Dissolved organic carbon in the South China Sea and its exchange with the Western Pacific Ocean

Kai Wu [a], Minhan Dai [a,*], Junhui Chen [a], Feifei Meng [a], Xiaolin Li [a], Zhiyu Liu [a], Chuanjun Du [a], Jianping Gan [b]

[a] State Key Laboratory of Marine Environmental Science, Xiamen University, Xiamen 361100, China
[b] Department of Mathematics and Division of Environment, Hong Kong University of Science and Technology, Kowloon, Hong Kong, China

ARTICLE INFO

Available online 18 June 2015

Keywords:
Total organic carbon
Kuroshio
Northern South China Sea
West Philippine Sea

ABSTRACT

Based on a large and high quality dataset of total organic carbon (TOC, an approximation of dissolved organic carbon) collected from three cruises in spring, fall and winter in 2009–2011, we examined the distribution of TOC and its seasonality in the oligotrophic regime of the Northern South China Sea (NSCS) as well as its exchanges with the West Philippine Sea (WPS) in the Northwest Pacific Ocean through the Luzon Strait, the only deep channel linking the South China Sea (SCS) and the Pacific Ocean. Surface TOC concentration in the slope and basin areas of the NSCS varied from 65 to 75 μmol L^{-1} with relatively high values in the northeast part (southwest of Taiwan Island) in spring, and in the eastern parts of the NSCS during fall and winter. The TOC inventory in the upper 100 m of the water column ranged from 6.0–7.5 mol m^{-2} with a similar distribution pattern as the surface TOC concentration. There were two most significant differences in the TOC profiles between the SCS and the WPS. One was in the upper 200 m, where more TOC was accumulated in the WPS; the other was in the intermediate layer at ~1000–1500 m, where the gradient of TOC concentration was still persistent below 1000 m in the SCS, a feature which did not exist in the WPS. At this intermediate layer, there also appeared an excess of TOC in the SCS as compared with that in the WPS. The TOC concentration below 2000 m in the SCS was identical to that in the Northwestern Pacific, both of which were ~40 μmol L^{-1} without significant difference among stations and seasons, suggesting that this deep water TOC was homogeneously distributed in the deep SCS basin owing to the fast replenishment of the deep water from the WPS. We adopted an isopycnal mixing model to derive the water proportion contributed respectively from the SCS and Kuroshio along individual isopycnal plane and examined the impact of the Kuroshio intrusion on the TOC in the NSCS. The upper 100 m TOC inventory in the NSCS was overall positively correlated with the Kuroshio water fraction, suggesting that the Kuroshio intrusion enhanced the TOC inventory thereby significantly influencing TOC distribution in the NSCS. Following the sandwich structure of water exchange through the Luzon Strait, with an inflow in the surface and deep layer but an outflow from the SCS in the intermediate layer, we conducted a first order estimation of the TOC transport fluxes based on the reported cross strait volume transport. The TOC transport flux was -107.1 ± 54.6, 54.7 ± 15.0 and -16.4 ± 13.1 Tg C yr^{-1} at the upper, intermediate and deep layer, respectively. Note that the positive sign means that the flux was from the SCS to the WPS. By integrating the three-layers, the total net transport flux of TOC through the Luzon Strait would be -68.8 ± 58.0 Tg C yr^{-1}. Because of the great spatial–temporal variability of the water flow across the Luzon Strait, these first order TOC flux estimates were subject to large uncertainty. Nevertheless, because the SCS is featured by higher DOC production, the exchange of these fluxes with the open ocean interior where DOC would have experienced more degradation would have important implications for both the microbial community in the ocean interior and overall carbon cycle in the SCS.

1. Introduction

Located in the continuity between the land and the ocean, ocean margins exchange waters and material with major ocean basins in a very dynamic and interactive way. Such exchange remains as a hard question both in terms of physical dynamics and biogeochemistry

* Corresponding author.
E-mail address: mdai@xmu.edu.cn (M. Dai).

http://dx.doi.org/10.1016/j.dsr2.2015.06.013
0967-0645/

(Huthnance et al., 2009 and references therein). Observational and modeling studies of water exchange between the marginal seas and the open ocean have been carried out at several locations including the Middle Atlantic Bight (Biscaye et al., 1994) the US western shelf (Jahnke et al., 2008) and the South China Sea (SCS; Tian et al., 2006; Qu et al., 2006; Hsin et al., 2012). These studies all point towards the complexity in mechanisms and fluxes of these water mass exchanges in time and space. It is even more challenging to resolve the material exchanges because many chemical constituents often exert large gradients between the ocean margin and the ocean interior induced by the difference in sources and the consumption in between. Dai et al. (2013) recently propose a new framework, the Ocean-dominated Margin (OceMar) characterized by dynamic interactions with the open ocean, which may provide non-local CO_2 sources thereby modulating the CO_2 fluxes in OceMars.

The SCS is the largest marginal sea of the Pacific Ocean, which exchanges with the West Philippine Sea (WPS) in the Northwestern Pacific Ocean through the Luzon Strait, the only deep water channel with a maximal sill depth of ~2200 m (Dai et al., 2009 and references therein). The water exchange across the Luzon Strait exhibits a "sandwich-like" flow pattern, with an inflow from the WPS in the upper and deeper layers but an outflow to the WPS in the intermediate layer (Chao et al., 1996; Li and Qu, 2006; Qu et al., 2006; Tian et al., 2006; Gan et al., 2006). The rapid replenishment of the SCS deep water from the WPS is maintained by fast ventilation with the shallower intermediate water, as well as a persistent net outflow at an intermediate depth (Chao et al., 1996; Chen et al., 2001; Li and Qu, 2006). Such a unique circulation pattern makes the SCS a perfect site to examine ocean margin–open ocean interactions.

Dissolved organic carbon (DOC) is the biggest organic carbon reservoir in the ocean, and is a critically important component in oceanic carbon cycling (Siegenthaler and Sarmiento, 1993). Ocean margins generally produce more organic carbon than they respire, and can significantly contribute organic carbon to fuel microbial metabolism in the deep open ocean (Dai et al., 2009 and references therein). However, our understanding of the DOC interaction between the marginal sea and open ocean is very limited. Our prior research has revealed that the intermediate outflow exports 3.1 ± 2.1 Tg C yr^{-1} of DOC from the SCS. Such export of excess DOC to the adjacent open ocean may represent an important pathway to sequestrate carbon within the SCS and a critically important carbon source of the interior Pacific Ocean, which would significantly contribute to fueling microbial metabolism in the Pacific Ocean Interior (Dai et al., 2009).

The present study will further such studies on the interactions between the SCS and WPS by reporting the full spectrum of DOC exchanges through the Luzon Strait based on a large and high quality dataset of total organic carbon (TOC, an approximation of DOC). Data were collected during three cruises that covered a large portion of the Northern SCS (NSCS). At the upper layer, we adopted an isopycnal mixing model (Du et al., 2013) to quantify the influence of the Kuroshio intrusion on the TOC inventory. At the intermediate and deep layers, the net exchange fluxes of TOC across the Luzon Strait were estimated based on the water mass exchange fluxes and TOC concentration gradients. Additionally, this study was aimed at better defining the seasonality of TOC within the SCS basin area, which has not been reported previously.

2. Materials and methods

2.1. The study area

The basin-scale surface currents in the SCS are driven to a significant extent by monsoons that result in a cyclonic circulation gyre during the northeast monsoon and an anti-cyclonic gyre during the southwest monsoon. As a consequence, the SCS basin is effectively isolated from terrestrial inputs and a wide area of the SCS basin is oligotrophic. Within this oligotrophic basin, both the biomass and primary productivity are believed to be dominated by the nutrient supply modulated by the strength of the seasonally reversing East Asian Monsoon (Liu et al., 2002, 2013). In winter, increased wind speed stimulates photosynthesis through strong mixing that entrains the nutrient-rich subsurface water to the upper layer; while in summer, the upper water column is highly stratified, which results in a reduction in biological productivity. Recently, Du et al. (2013) quantify that the degree of the Kuroshio intrusion into the SCS also significantly impacts the upper SCS nutrient inventory.

2.2. Sampling and analysis

TOC samples were collected during winter (Dec., 2009–Jan., 2010), fall (Oct.–Nov., 2010) and spring (Apr.–Jun., 2011) covering nearly the entire NSCS basin and the Luzon Strait. We focused on a region from 111 to 120°E and from 18 to 22°N, roughly the 200 m isobaths in the zonal direction (Fig. 1). In this study, we considered only stations with water depth >200 m, where TOC concentration was not significantly influenced by terrestrial sources.

Samples were collected in duplicate using acid cleaned 12 L Niskin bottles attached to the CTD rosette as previously described (Dai et al., 2009). Samples were not filtered and were stored in precombusted EPA vials at -20 °C until analysis. Here, we used TOC as an approximation of DOC given the fact that particulate organic carbon (POC) concentrations based on our parallel study represented on average only ~4% of TOC (Cai et al., 2015). TOC was measured using a Shimadzu TOC-V analyzer. A four-point calibration curve was obtained by injecting working solutions of potassium hydrogen phthalate, which was freshly prepared every two days. TOC concentration was determined by subtracting the running blank from the average peak area of the samples (injected 3–4 times) and dividing the subtraction by the slope of the calibration curve. The running blank was determined as the average of the peak area of the Milli-Q water acidified with H_3PO_4. Low carbon water and deep sea water, provided by Dr. Hansell's laboratory at the University of Miami, were used for quality assessment of our measurements. The coefficient of variation on the analysis of our replicate measurements was ~2%. The standard deviation of our long term replicate measurements on the reference deep sea water was ± 0.8 μmol L^{-1}, which was used as an index of our analytical precision.

2.3. Isopycnal mixing model

In order to quantify the impact of the Kuroshio intrusion on the TOC inventory in the NSCS, a well validated isopycnal model (Du et al., 2013) was adopted. Using this model, we calculated the mixing ratios contributed by the different water masses along the isopycnal plane. The model assumed that the isopycnal mixing rate was much faster than the diapycnal mixing rate and so the effect of diapycnal mixing could be negligible. Within the SCS, we estimated the isopycnal mixing rate of TOC to be 6.0×10^{-3} mmol m^{-2} s^{-1}, which was three orders of magnitude larger than the diapycnal mixing rate of $\sim 1.0 \times 10^{-6}$ mmol m^{-2} s^{-1}.

Details of the application of the isopycnal mixing model are introduced by Du et al. (2013). For any in situ observed water parcel shown in the T–S diagram in Fig. 2a, the proportional contributions of SCS and the Kuroshio along the individual isopycnal surface can be calculated (Eq. (3)) based on the conservation of salinity or potential temperature (Eqs. (1) and (2)):

$$R_{SCS}\theta_{SCS} + R_{Kuroshio}\theta_{Kuroshio} = \theta \text{ or } R_{SCS}S_{SCS} + R_{Kuroshio}S_{Kuroshio} = S \quad (1)$$

$$R_{SCS} + R_{Kuroshio} = 1 \quad (2)$$

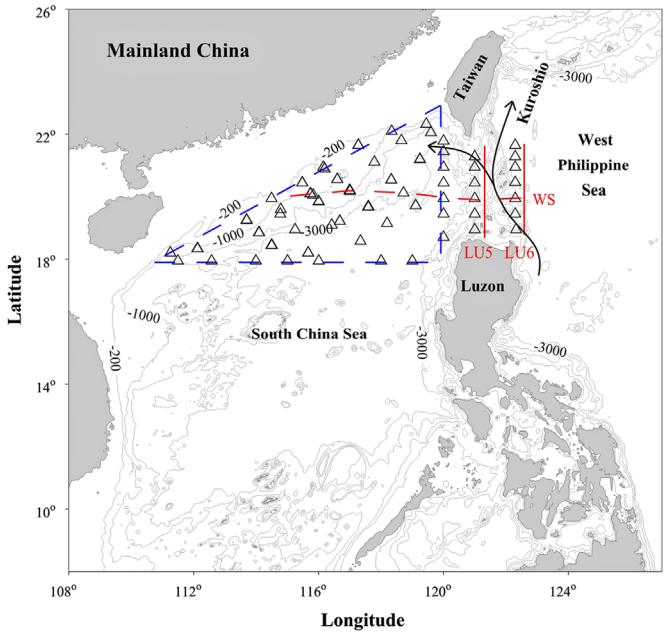

Fig. 1. Map of the NSCS showing its topography and the locations of the sampling stations (triangles). Two meridional sections along the Luzon Strait are highlighted with solid vertical red lines (i.e. LU6 and LU5) and the dashed horizontal red line denotes a zonal section (WS) across the Luzon Strait to the NSCS basin during the spring cruise. The black line is the Kuroshio Current and its branch into the South China Sea. Note that the estimation of the area-integrated TOC inventory presented in the text was calculated from the stations in the blue dashed area of triangles.

$$R_{Kuroshio} = \frac{\theta - \theta_{SCS}}{\theta_{Kuroshio} - \theta_{SCS}} \text{ or } R_{Kuroshio} = \frac{S - S_{SCS}}{S_{Kuroshio} - S_{SCS}} \quad (3)$$

$R_{Kuroshio}$ is the Kuroshio water proportion in the mixed water, and R_{SCS} represents the SCS water proportion; $\theta_{Kuroshio}$and $S_{Kuroshio}$ are the endmember values of potential temperature (θ) and salinity for the Kuroshio water, while θ_{SCS} and S_{SCS} are the endmember values of the potential temperature (θ) and salinity for the SCS water proper. Following Du et al. (2013) salinity was chosen for water fraction estimation in the upper 50 m where θ was affected by solar radiation heating. However, at deeper layers, θ was used for the estimation, because of its higher sensitivity than salinity.

With the derived water fractions, the TOC concentrations of each water parcel in the central NSCS (Fig. 2b) due to conservative mixing along the isopycnal surface between the SCS water proper and the Kuroshio water proper could be calculated using:

$$TOC_{Model} = TOC_{SCS}R_{SCS} + TOC_{Kuroshio}R_{Kuroshio} \quad (4)$$

TOC_{Model} is the TOC concentration solely due to conservative mixing between the SCS water and the Kuroshio water. TOC_{SCS} and $TOC_{Kuroshio}$ are the endmember values of the SCS and the Kuroshio water derived by fitting the TOC profiles of the SCS and Kuroshio waters proper against potential density. TOC profiles of the SCS and Kuroshio waters proper were chosen based on the T–S plot shown in Fig. 2a.

2.4. Estimation of TOC inventory

We estimated the station-integrated and area-integrated TOC inventories in the central NSCS with the field observation data. The former was calculated by integrating TOC concentrations in the upper 100 m of the water column at each station. The latter was obtained by integrating the station-integrated TOC inventories over the entire study area via spatial interpolations, for which the Inverse Distance Square method was applied (Du et al., 2013).

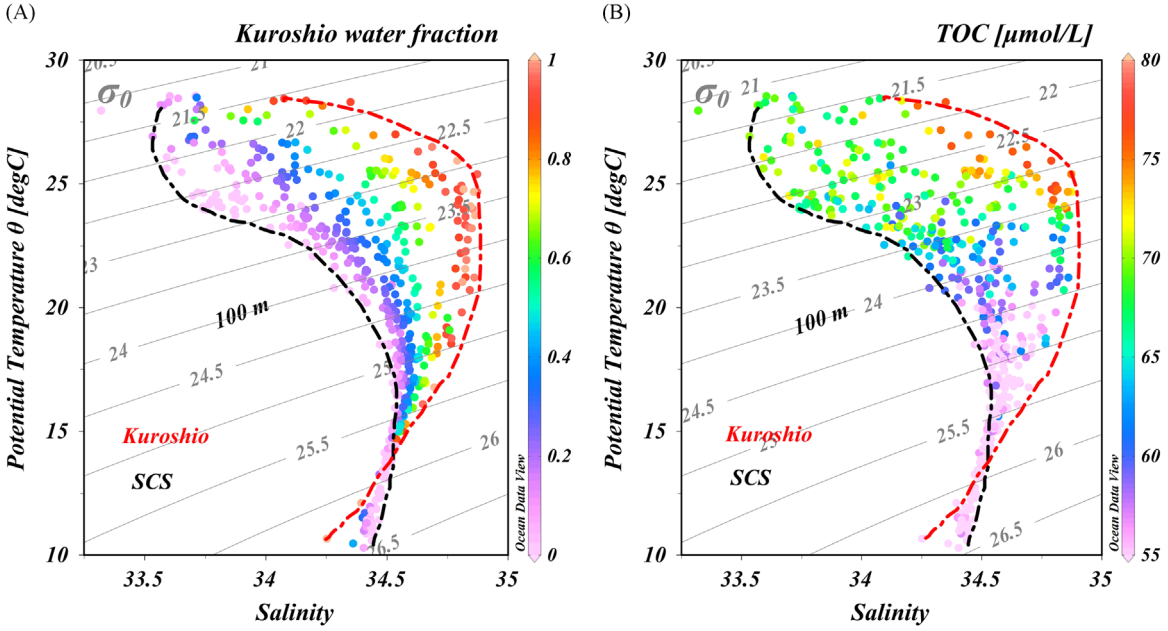

Fig. 2. Potential temperature versus salinity plots in the upper 400 m for the sampling stations in the central NSCS and WPS superimposed by (a) the Kuroshio water fraction (R_k) derived from the isopycnal model that was redrawn after Du et al. (2013); and (b) the field observed TOC concentrations. The dark dot–dash line denotes the typical Kuroshio water, while the red dot–dash line denotes the typical SCS water.

3. Results

3.1. Hydrography

The hydrology of the surface water (<200 m) is introduced in Du et al. (2013). Briefly, as shown in the T–S diagram (Fig. 3) there was a distinct difference in hydrology between the central NSCS and the Kuroshio in the upper 200 m of the water column, the latter being indicated by data points collected in sections LU5 and LU6. At $\sigma_\theta < 25.8$, the Kuroshio water tended to have higher salinity than the SCS water. All of the surface water ($\sigma_\theta < 25.8$) collected during our cruises was a mixture of the SCS and Kuroshio proper with varied combinations of both. At the subsurface, the T–S distribution pattern in sections LU5 and LU6 mostly reflected mixtures of the WPS and the SCS waters proper.

3.2. TOC distribution in the central NSCS

The horizontal distribution of TOC in the upper 100 m of the NSCS during the three cruises is shown in Fig. 4. The range of surface TOC concentrations was 65–79 μmol L^{-1} in spring, and 68–73 μmol L^{-1} in fall and winter. During spring, relatively high surface TOC concentrations were observed in the Kuroshio water (sections LU5 and LU6) and in the area near the southwest of Taiwan Island and along the shelf break. At 50 and 100 m, low TOC concentrations (<56 μmol L^{-1}) were observed in the central basin during spring. This region was characterized by low sea water temperature and high salinity (data not shown), where the sea surface height anomaly also showed low values (~ -10 cm) (data from http://eddy.colorado.edu/ccar/ssh/nrt_global_grid_viewer) indicating possible cyclonic eddy processes that brought low TOC waters from depth. Meanwhile, high TOC concentrations were also observable in the Kuroshio water and near the southwest of Taiwan Island at the 50 and 100 m depth horizons. In fall and winter, it was apparent that TOC concentrations were relatively higher in the eastern regions than those in the western regions of the NSCS at 5, 50 and 100 m.

3.3. TOC inventory in the upper 100 m

The station-integrated TOC inventory in the upper 100 m of the central NSCS and Kuroshio during different seasons is shown in Fig. 5. In spring, the TOC inventory ranged from 6.0–7.5 mol m^{-2}. The high inventory (>7.0 mol m^{-2}) appeared in the WPS and the northeastern part near Taiwan and low inventories of <6.5 mol m^{-2} were in the central four stations that were influenced by the cyclonic eddy. During fall and winter, the TOC inventory was higher in the eastern part (>6.8 mol m^{-2}), but lower in the western part. The annual averaged TOC inventory in the central NSCS was ~ 6.7 mol m^{-2}, which was significantly lower than that in the Kuroshio (7.5 mol m^{-2}), implying that the Kuroshio intrusion would increase the TOC inventory in the upper 100 m of the NSCS. Taking the central NSCS as a whole, the area-integrated TOC inventory was highest in fall (~ 25.2 Tg) while it was 5.6% and 6.3% lower in spring (~ 23.8 Tg) and winter (~ 23.6 Tg). Apart from the cyclonic eddy, the seasonal variation of the area-integrated TOC inventory might have been primarily induced by two other processes. One was related to the different extent of Kuroshio intrusion, which brought in higher TOC waters. Meanwhile, the enhanced primary production in the SCS basin during fall and winter, due to the strong vertical mixing that entrained the nutrient-rich water to the upper layer (Chen and Chen, 2006) could also have elevated the TOC production in the upper SCS. Given that the SCS water in fall was less influenced by the Kuroshio water as shown in the T–S diagram (Fig. 3) biological production might thus be the major reason causing the highest TOC inventory in fall. However, the mechanisms for the high production of TOC in fall are still unclear, and require further studies.

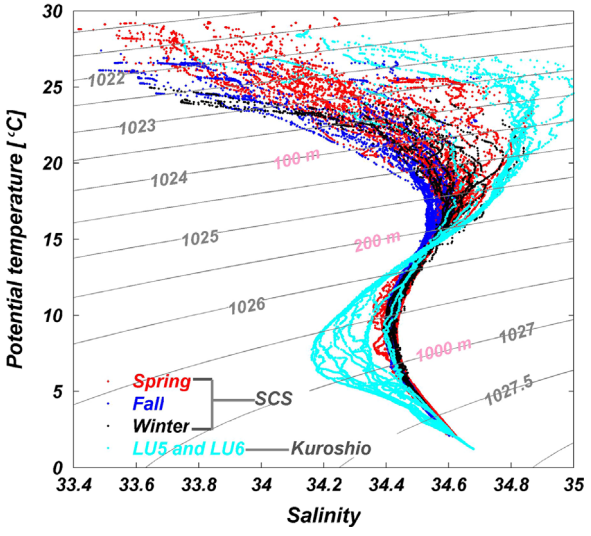

Fig. 3. Potential temperature (°C) versus salinity plots (T–S) diagram for the sampling stations during spring, fall and winter cruises (cyan dots: LU5 and LU6 sections during spring; pink dots: spring; blue dots: fall; and black dots: winter). The plots were redrawn from the data reported in Du et al. (2013).

3.4. Comparison of TOC distributions between the NSCS and the WPS

3.4.1. TOC distribution across the Luzon Strait

The Luzon Strait is the portal for the transfer of Kuroshio water to the SCS and water exchange through the Luzon Strait is well documented (Yang et al., 2010; Zhao et al., 2014; Qu et al., 2006). Fig. 6 shows the transectional distribution of potential temperature, salinity and TOC along roughly a zonal transect, at 20°N from the WPS across the Luzon Strait, which extended into the SCS and was named Transect WS. In the upper 200 m, the potential temperature in the WPS was higher than that in the NSCS basin, suggesting that surface water was more stratified in the WPS. Salinity at 50–200 m in the WPS also displayed high values (~ 34.872), which were identical to the value of typical Kuroshio subsurface water (Shaw and Chao, 1994). Meanwhile, TOC concentration at the same depth in the WPS was higher than in the NSCS basin.

The distribution of salinity showed a minimum core at ~ 500 m in the NSCS and the WPS. At 1000–1500 m in the Luzon Strait, the uplift of the isothermals indicated the upwelling of the deep water. Below 2000 m, the potential temperature, salinity and TOC in the NSCS were the same as those in the WPS, confirming that the source of the deep water in the SCS was from the WPS (Qu et al., 2006). It was noted that TOC concentrations at 1000–1500 m in the NSCS basin were higher than those in the WPS.

3.4.2. SCS vs WPS

3.4.2.1. In the upper layer. As shown in Fig. 7a, TOC concentration in the upper layer (0–100 m) in the SCS ranged from 55 to 70 μmol L^{-1}, which was comparable with previous observations (Dai et al., 2009). As compared to the SCS, TOC concentration (60–79 μmol L^{-1}) in the upper 100 m, or at $\sigma_\theta < 23.5$ along Section LU 6 in the WPS, was higher (Fig. 7b). As shown in Fig. 6a, the potential temperature in the upper layers (50–200 m) of the SCS was lower than that in the WPS. Thus, the presence of colder water in the SCS indicated that upward advection of deep colder water must have happened and this process was capable of bringing up TOC-depleted deep waters, which would dilute TOC concentration

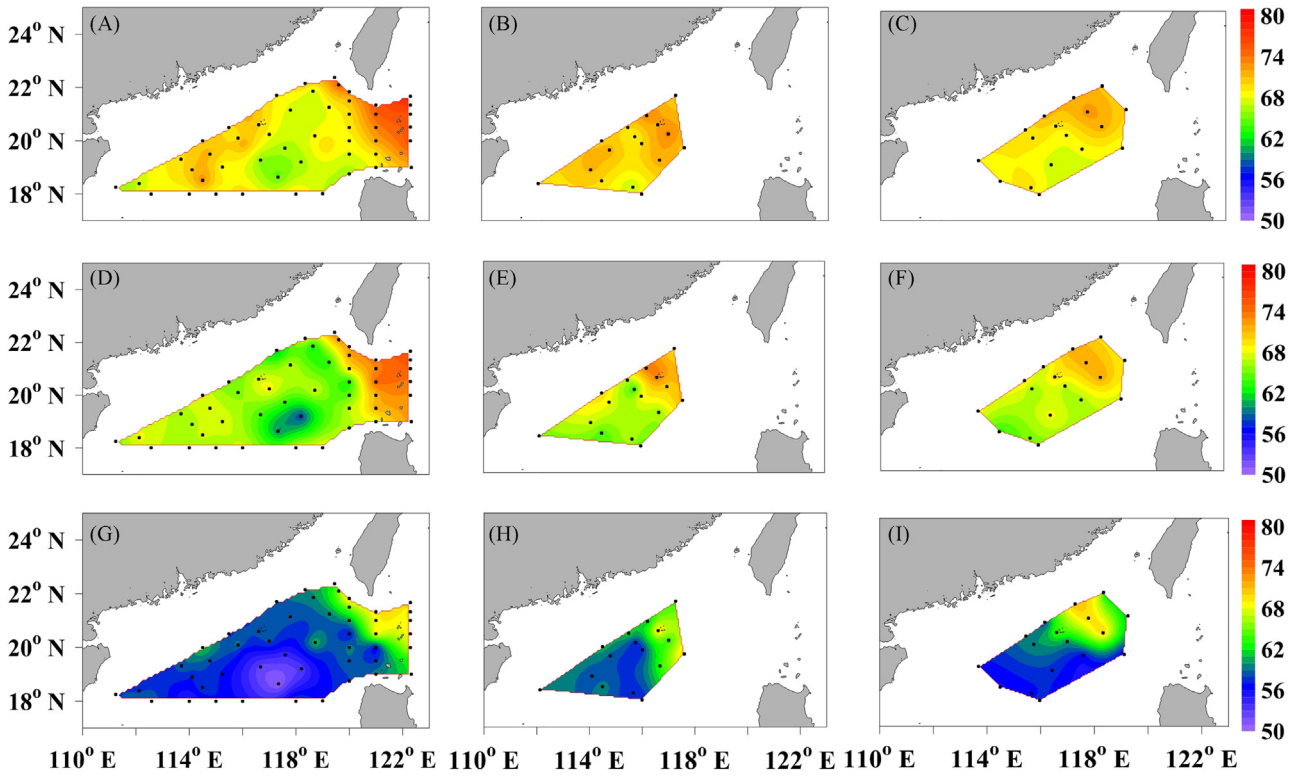

Fig. 4. Iso-depth distribution of TOC at depths of 5 (a, b, c), 50 (d, e, f) and 100 m (g, h, i) in the central NSCS and the Kuroshio during spring (a, d, g), fall (b, e, h) and winter (c, f, i). Note that the sampling in the Kuroshio was only in spring.

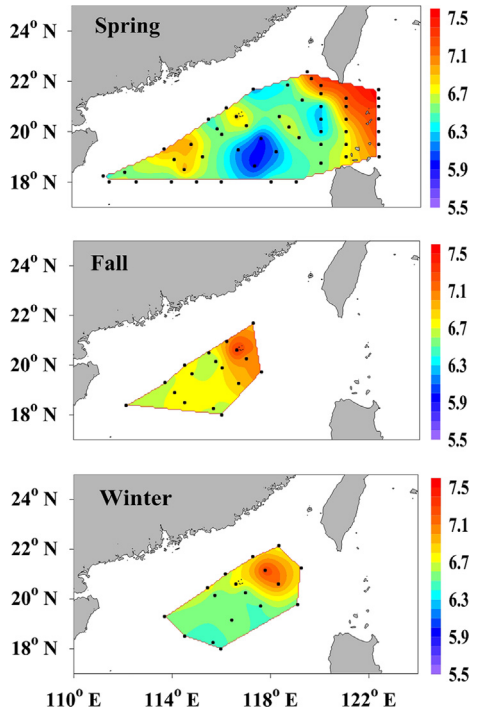

Fig. 5. Station-integrated TOC inventory (mol m^{-2}) in the upper 100 m of the central NSCS and Kuroshio during spring, fall and winter.

in the upper layers. On the other hand, Shiah et al. (1998) report that the lower availability of inorganic nutrients limits the growth of bacteria and results in the accumulation of DOM in the upper layer of the WPS. The bacterial production data derived during the same cruises (unpublished data from Dr. Chen B.Z.) indeed showed significantly lower bacterial production in the surface layer of the Kuroshio (0.019 μg C L^{-1} d^{-1}) than in the NSCS basin (0.045 μg C L^{-1} d^{-1}). In this context, the intrusion of the Kuroshio would increase the TOC concentration and inventory in the upper 100 m of the NSCS.

3.4.2.2. In the intermediate layer. In the intermediate water (~1000–1500 m, σ_θ=27.2–27.6) Dai et al. (2009) report an excess of TOC between the SCS and the Northwestern Pacific Ocean. In the present study, at 1000–1500 m, TOC concentrations at all stations from all the cruises in the SCS basin and the WPS were 42.9 ± 0.9 and 40.3 ± 0.6 μmol L^{-1}. The enrichment of TOC (2.6 ± 1.0 μmol L^{-1}) was similar to that reported by Dai et al. (2009) (3.3 ± 1.1 μmol L^{-1}) and was statistically significant given our measurement error of ± 0.8 μmol L^{-1}. The sources of this excess TOC in the SCS intermediate water were unclear but might result from the breakdown/dissolution of sinking particles (Dai et al., 2009) and/or of particles through lateral transport from the shelf. Importantly, the fact that the vertical gradient in TOC concentrations continued down to 2000 m in the SCS (Fig. 7) which is not seen in other major ocean basins, has significant implications.

3.4.2.3. In the deep layer. TOC concentration below 2000 m in the SCS was almost identical to that in the Northwestern Pacific, both of which were ~40 μmol L^{-1} (Dai et al., 2009). This deep water TOC appeared to be homogeneously distributed in the deep SCS basin showing no significant difference among stations and seasons, suggesting again the fast replenishment of the deep water from the WPS as previously noted (Qu et al., 2000; Broecker et al., 1986).

In summary, there were two most significant differences in the TOC profiles between the SCS and the WPS. One was in the surface layer, where more TOC accumulated in the WPS; the other in the intermediate layer, where the gradient of TOC concentration was still persistent below 1000 m in the SCS, a feature of which did not exist in the WPS. Combining the water exchange through the

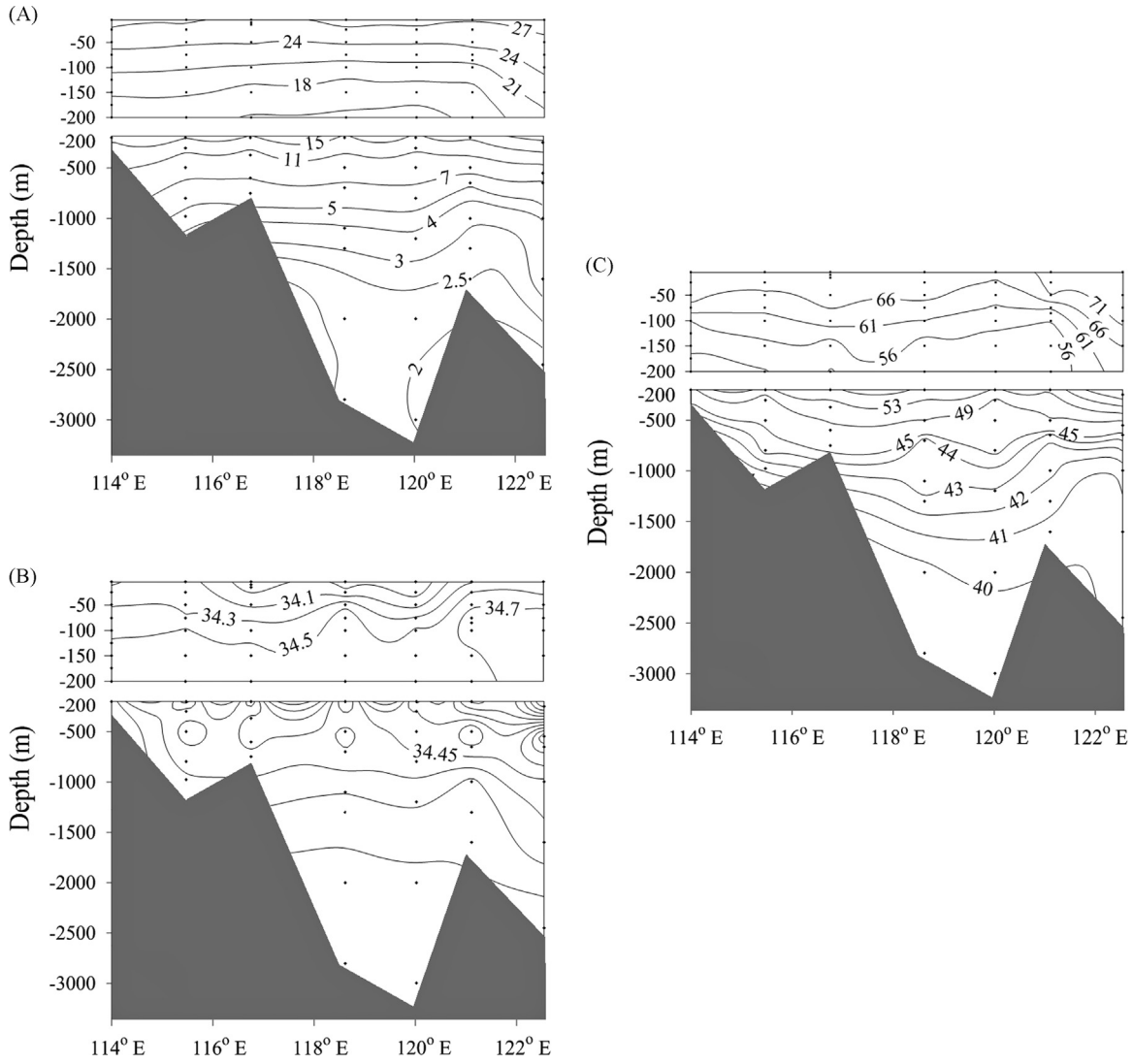

Fig. 6. Distribution of potential temperature (a), salinity (b) and TOC concentration (c) along section WS (the section beneath the dashed red line in Fig. 1) during the spring cruise.

Luzon Strait, the exchange of TOC and its significance is discussed below.

4. Discussion

4.1. The impact of Kuroshio intrusion on the TOC inventory in the upper 100 m of the NSCS

The station-integrated Kuroshio water fraction (R_{IKW}) in the upper 100 m (Fig. 8) could be obtained by integrating the Kuroshio water fraction (R_k) in each water layer. The spatial distribution of R_{IKW} is introduced in Du et al. (2013). Briefly, in spring, the R_{IKW} was high (above 0.4) in the region near to the southwestern part of Taiwan and at some stations along the slope in the western portion of the NSCS. During fall and winter, the R_{IKW} in the eastern part of the NSCS (>0.2) was higher than that in the western part (<0.1). Nevertheless, from the spatial distribution of R_{IKW} during the different cruises, the influence of Kuroshio water in the NSCS was clear. Compared to that in fall, the R_{IKW} in the central NSCS was slightly higher in spring and winter, suggesting stronger influence of the Kuroshio intrusion in spring and winter. This was consistent with the results indicating that the Kuroshio intrusion reached its maximum extent in spring (Chu and Li, 2000). Similarly, we calculated the station-integrated Kuroshio TOC fraction (R_{IKTOC}) as follows:

$$R_{IKTOC} = \frac{I_{KTOC}}{I_{TOC}} = \frac{\sum_{Z=0}^{Z=100m} R_K \times TOC_K}{\sum_{Z=0}^{Z=100m} (TOC_{Model})} \quad (5)$$

where I_{TOC} is the station-integrated inventory of model predicted TOC in the upper 100 m of the central NSCS, and I_{KTOC} is the station-integrated inventory of TOC contribution from the Kuroshio water. The distribution of R_{IKTOC} (Fig. 8) was similar to the R_{IKW}, showing a high Kuroshio TOC contribution in the eastern part of the NSCS. The average value of R_{IKTOC} for all stations in spring and winter was 0.31 ± 0.1 and 0.30 ± 0.2, higher than that in fall (0.1 ± 0.08). Although we lacked the summer data, the R_{IKTOC} value in summer was expected to be small, because the prevailing southwest monsoon would diminish the Kuroshio intrusion (Shaw, 1991).

The comparison between the field measured and the model predicted TOC concentrations is shown in Fig. 9a. Overall, the model predictions agreed well with the field measurements. The dots that fell outside the standard deviation domains might suggest the biological alteration of TOC in the upper 100 m of the NSCS. As shown in Fig. 9b, the field estimated TOC inventory was

overall positively correlated with the Kuroshio water proportion during spring ($R^2=0.36$, $P<0.0001$), fall ($R^2=0.6$, $P<0.0001$) and winter ($R^2=0.68$, $P<0.0001$). During spring and winter, the linear regression slopes were almost equal to 1, which was the same as the value of the theoretical mixing line between the SCS and the Kuroshio. This suggested that the Kuroshio intrusion was the major process controlling the TOC inventory in the upper 100 m during spring and winter. However, the linear regression slope in fall (1.7) was higher than that of the theoretical mixing line, revealing biological production of TOC in the upper 100 m of seawater.

In order to assess the accumulation of the TOC inventory due to the Kuroshio intrusion, we calculated its increase in terms of the area-integrated TOC inventory over the upper 100 m of the central NSCS

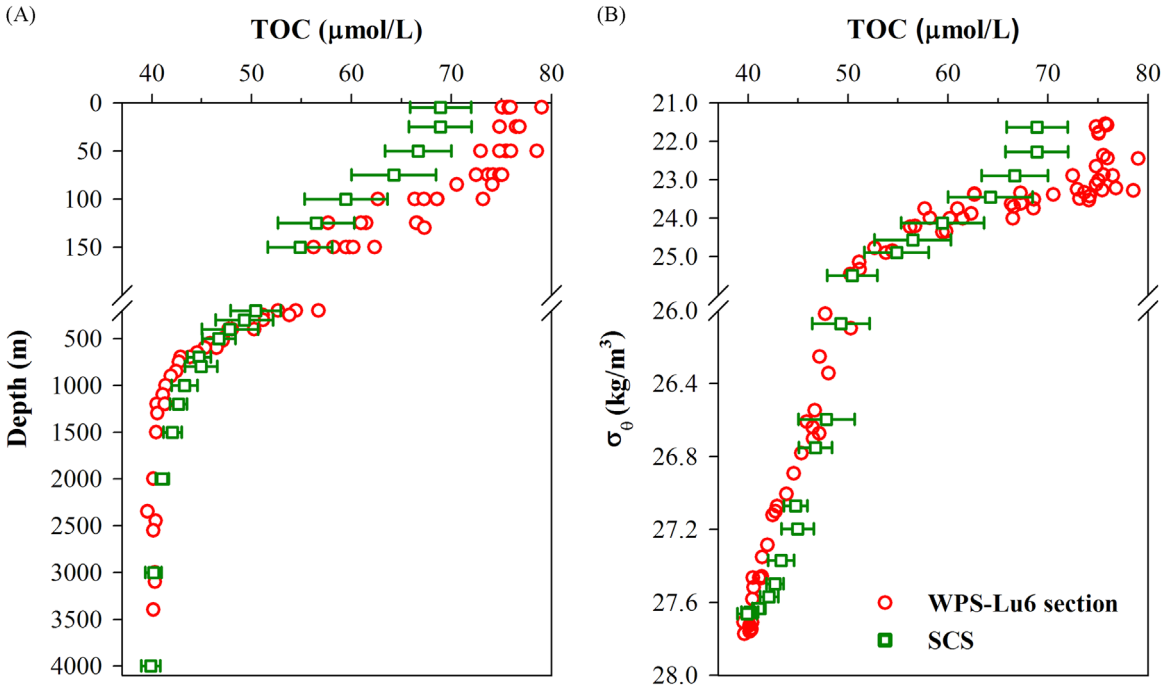

Fig. 7. (a) Depth profiles of averaged TOC from all the stations in the NSCS basin during all the cruises (green squares) and from the LU6 section in the WPS during the spring cruise (red circles). Standard deviations are shown as error bars. (b) Potential density (σ_θ) versus TOC for all corresponding samples in Fig. 7a.

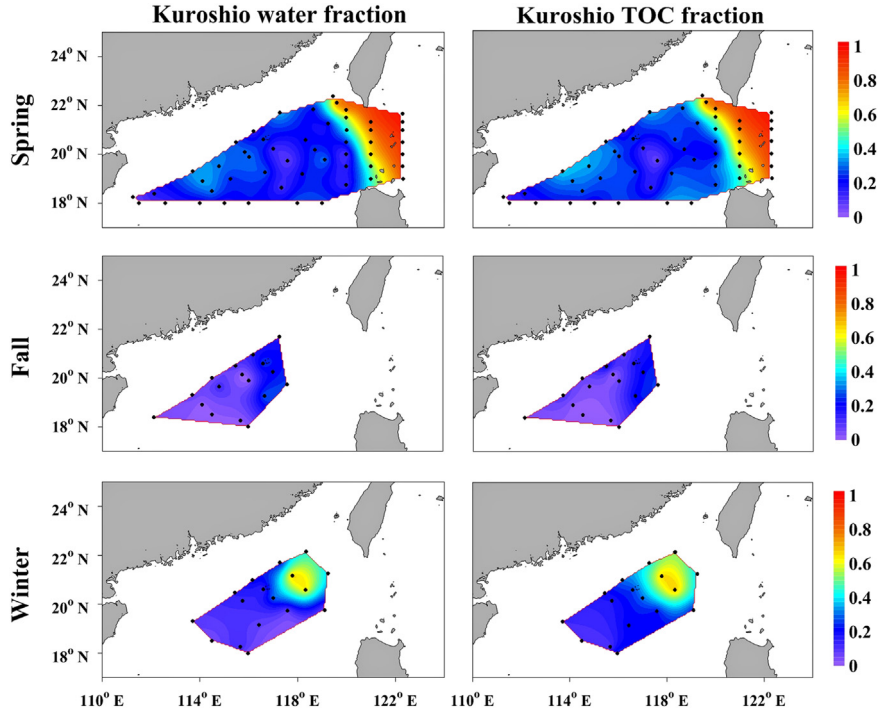

Fig. 8. Station-integrated Kuroshio water fraction and Kuroshio TOC fraction in the upper 100 m of the central NSCS and Kuroshio during spring, fall and winter.

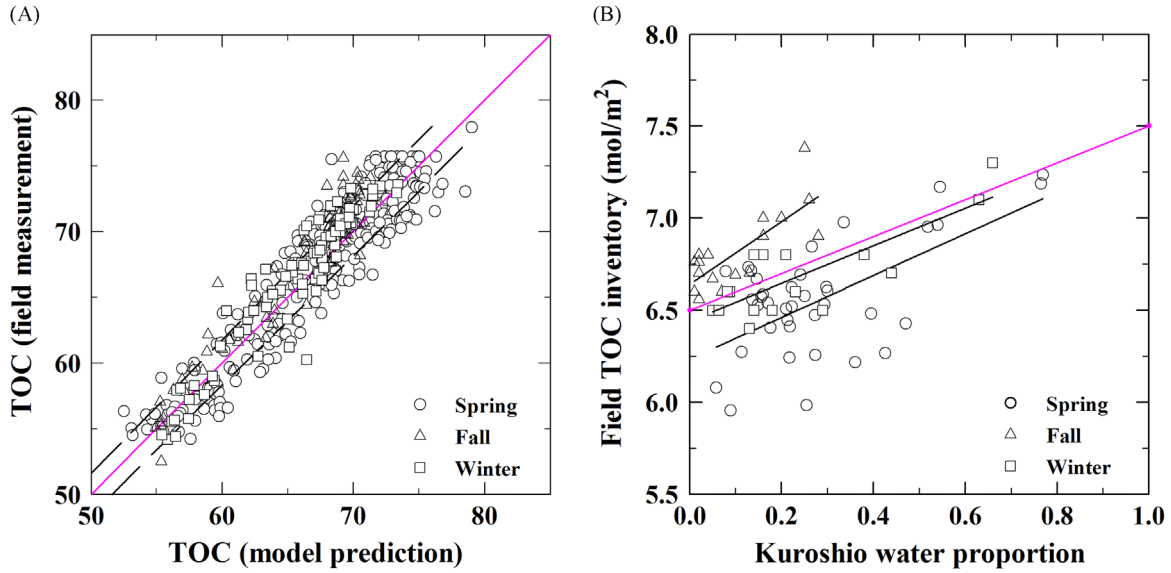

Fig. 9. (a) The field measured TOC concentrations versus the model prediction in the upper 100 m in the central of the NSCS (left) (the pink line is the 1:1 line, while the dashed black lines are the standard deviation); and (b) the relationship between the field observed TOC inventory and the station-integrated Kuroshio water proportion. The pink line is the theoretical mixing line constructed using the TOC inventory of the SCS and Kuroshio end-members (~6.5 mol m^{-2} in the NSCS and ~7.5 mol m^{-2} in the Kuroshio, which was obtained by assuming that the Kuroshio water fraction in the upper 100 m was the same).

$$K_{TI} = \sum^{area} \left(\sum_{z=0m}^{z=100m} (N_K) - \sum_{Z=0m}^{z=100m} (N_S) \right) \quad (6)$$

Here, N_S is the SCS endmember TOC concentration, and N_K is the model predicted TOC concentration. Assuming the study area was under a steady state on intra-seasonal time scale, the calculated K_{TI} values in spring, fall and winter were 1.5, 0.9 and 1.1 Tg. Accordingly, the Kuroshio intrusion would increase by $7 \pm 4\%$, $4 \pm 2\%$ and $5 \pm 3\%$ of the TOC inventory in the NSCS during spring, fall and winter. We also calculated that the Kuroshio intrusion accounted for $\sim 93 \pm 10\%$, $\sim 52 \pm 20\%$ and $\sim 80 \pm 14\%$ of the increase in inventory during spring, fall and winter, whereas the residual of the increase might be attributed to biological metabolism. During spring and winter, the Kuroshio intrusion was the dominant factor in enhancing the TOC inventories, while biological production might also be important in controlling the TOC inventories in fall. It should be pointed out that these assessments were referenced to spring 2011, while our three cruises spanned 2009–2011. Therefore, our estimated increase at seasonal levels assumed no interannual variations in the Kuroshio intrusion into the SCS, and this was not always true.

It should be pointed out that the Kuroshio TOC might be biodegradable in the SCS over the seasonal time scale. Considering this, our estimation in the station-integrated Kuroshio TOC fraction (R_{IKTOC}) and Kuroshio induced increase in the area-integrated TOC inventory (K_{TI}) in the SCS based on the conservation of the Kuroshio TOC should be regarded as the upper limits.

4.2. Biological production of TOC in the upper 100 m of the central NSCS

Although the model predicted TOC concentrations and the field measurements showed an overall agreement in the upper 100 m of the central SCS, small though observable departures did exist. This is because during the mixing of the SCS and the Kuroshio waters proper, biologically mediated degradation and/or production of TOC would occur, in particular in the upper layer, the net change of which is defined here as ΔTOC, or the difference between the model prediction and field measurements. Given the small values of ΔTOC, it is important to well constrain the uncertainty when we report the ΔTOC.

It was clear that the uncertainty in assessing ΔTOC was dependent on the errors associated with TOC_{Model} and TOC_{Field}. Here, the uncertainty of TOC_{Model} was estimated using Eq. (7)

$$\delta_{TOC_{Model}} = \sqrt{(TOC_K - TOC_{SCS})^2 \delta_{R_K}^2 + R_K^2 \delta_{TOC_K}^2 + (1 - R_K)^2 \delta_{TOC_{SCS}}^2} \quad (7)$$

where TOC_{SCS} and TOC_K are the TOC concentrations of the SCS and Kuroshio end-members, R_K is the Kuroshio water fraction, and δ_{R_K}, δ_{TOC_K} and $\delta_{TOC_{SCS}}$ are the respective uncertainties of the Kuroshio water fraction and the TOC concentrations of the SCS and Kuroshio endmembers. The uncertainty of ΔTOC could therefore be calculated using Eq. (8)

$$\begin{aligned} \delta_{\Delta TOC} &= \sqrt{(\delta_{TOC_{Model}})^2 + (\delta_{TOC_{Field}})^2} \\ &= \sqrt{(TOC_K - TOC_{SCS})^2 \delta_{R_K}^2 + R_K^2 \delta_{TOC_K}^2 + (1 - R_K)^2 \delta_{TOC_{SCS}}^2 + (\delta_{TOC_{Field}})^2} \end{aligned} \quad (8)$$

where $\delta_{TOC_{Field}}$ is the uncertainty of the TOC measurement.

As shown in Eq. (8), the uncertainty of ΔTOC was from $((TOC_K - TOC_{SCS})^2 \delta_{R_K}^2, R_K^2 \delta_{TOC_K}^2, (1 - R_K)^2 \delta_{TOC_{SCS}}^2$ and $(\delta_{TOC_{Field}})^2)$. Here, δ_{R_K} was estimated by Du et al. (2013) using a more conservative tracer, Ca^{2+}, and $(TOC_K - TOC_{SCS})^2 \delta_{R_K}^2$ could thus be estimated as 0.2. The uncertainty of the TOC concentrations of the SCS and the Kuroshio endmembers resulting based on the fitting of the TOC profiles of the SCS and the Kuroshio waters proper were up to 1.3 μmol L^{-1} and 1.9 μmol L^{-1}. $(1 - R_K)^2 \delta_{TOC_{SCS}}^2$ and $R_K^2 \delta_{TOC_K}^2$ could thus be estimated as 0.3–1.7 and 0–1.3 due to the range of Kuroshio water fraction (0–0.6) in the mixed water in the NSCS basin. The uncertainty of the TOC measurement $((\delta_{TOC_{Field}})^2)$ was 0.6. Accordingly, we could estimate that the uncertainty of ΔTOC was 1.5–1.6 μmol/L, and the maximum uncertainty (1.6 μmol/L) of ΔTOC was shown in the pink shadow in Fig. 10.

As shown in Fig. 10, the majority of the departures occurred in the upper euphotic zone where TOC concentrations were higher than 60 μmol L^{-1}. A scatter distribution ranging from −8 to

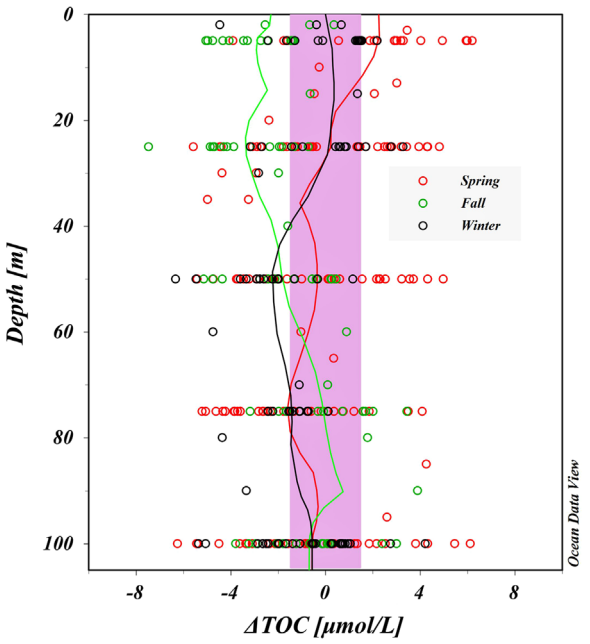

Fig. 10. Biologically altered TOC (ΔTOC) versus depth (m) in the upper 100 m of the NSCS. The solid lines represent the moving average, and the pink shadow is the uncertainty of ΔTOC.

8 μmol L^{-1} was found in the upper 100 m of the central NSCS. The majority of these data could be grouped within ± 6 μmol L^{-1}. As shown by the seasonally moving average line, ΔTOC was negative and fell out of the standard deviation domain in the upper 50 m during fall and between 50 m and 75 m during winter, suggesting a net production of TOC during fall and winter. Such net TOC production was consistent with the fact that the primary production was generally higher in fall and winter in the SCS, compared to the other seasons. In spring, ΔTOC was around zero, suggesting no significant net biological consumption or production of TOC.

The average ΔTOC in the upper 100 m was -1.8 ± 0.3 and -0.8 ± 0.2 μmol L^{-1} in fall and winter respectively. Assuming our study area was under a steady state on a seasonal time scale with an average of 90 days in fall and winter, we calculated that the net TOC production rate in fall and winter would be 24 ± 4 and 11 ± 3 mg C m^{-2} d^{-1}. Based on the same model, Du et al. (2013) estimate that the new production rate in winter is 88.8 mg C m^{-2} d^{-1}. Thus, the ratio of TOC production to new production in the basin of the NSCS in winter was 12%, which was close to the average value of 17% in the open ocean (Hansell and Carlson, 1998).

TOC accumulates in the upper ocean as part of new production (Hansell and Carlson, 1998). In winter, the presence of net TOC production was consistent with the enhanced new production estimated using the net nutrient consumption shown in Du et al. (2013) and Chen and Chen (2006). However, net TOC production was still persistent in fall without net nutrient consumption. This was probably because there were other sources for supplying nutrients in fall, for example the atmospheric deposition observed in the NSCS during the period of the northwestern monsoon (Chen et al., 2001; Lin et al., 2007). In spring, the new production rate is similar to that in winter (Du et al., 2013) whereas no significant net TOC production was observed in the present study. This may imply that the consumption and production of TOC was tightly coupled in spring. Chen et al. (2012) report relatively higher bacterial abundance in the NSCS basin in spring than in winter, suggesting that more TOC was consumed to support bacterial growth.

4.3. TOC transport fluxes through the Luzon Strait

Although the sandwich structure of the flow pattern through the Luzon Strait is relatively well known (Chao et al., 1996; Qu et al., 2000; Tian et al., 2006), constraint of the water fluxes remained difficult, owing to their great spatial and temporal variations. During the past decade, a number of studies either based on direct field observations or modeling have been devoted to studying the water exchange flux via the Luzon Strait, and it has become possible to estimate the material transport fluxes.

Using the same calculation method as in previous studies (Krom et al., 2004; Gomez, 2003; Civitarese et al., 1998), the net TOC transport fluxes through the straits were estimated as the difference between the inflow and outflow flux. In a simplified way, the calculation of the net TOC transport flux (F_{Net}) through the Luzon Strait could be expressed as in Eq. (9)

$$F_{Net} = F_{Outflow} - F_{Inflow} = f_{Eastward} C_{Eastward} - f_{Westward} C_{Westward} \quad (9)$$

Here, $f_{Eastward}$ and $f_{Westward}$ denote the eastward (outflow) and westward (inflow) volumetric rate of transport through the Luzon Strait; and $C_{Eastward}$ and $C_{Westward}$ are TOC concentrations in the outflow and inflow waters. The positive F_{Net} meant a net export rate of TOC from the SCS to the WPS, and the negative meant a net input of TOC into the SCS.

The observational TOC data were very sporadic in both time and space, we thus adopted the predicted TOC concentrations using the isopycnal mixing model to better define the TOC concentrations in the outflow and inflow waters. Using the three-layer model of water exchanges through the Luzon Strait, we estimated the net transport flux of TOC in each layer, based on the water fluxes reported and the TOC concentrations predicted. Then, the total net TOC exchange flux through the Luzon Strait was calculated by summing the net flux of TOC in each layer.

4.3.1. Net TOC transport flux through the Luzon Strait in the upper layer

In the upper layer (~500 m), due to the seasonal reversal of the East Asia monsoon that can highly influence intrusion of the Kuroshio (Hsin et al., 2012) the net volume exchange rate has large variability, showing strong westward transport in winter but much weaker transport in summer (Shaw, 1991; Qu et al., 2000). The annual average of the net water flux is westward, ranging from -0.8 to -10.3 Sv (Yuan et al., 2008; Liao et al., 2008).

The depth-averaged TOC concentration of the upper layer in the westward or eastward flow water could be calculated using Eq. (10)

$$\begin{aligned} C_{depth-averaged} &= \frac{\sum_{Z=0}^{Z=500m} TOC_{Model}}{500} \\ &= \frac{\sum_{Z=0}^{Z=500m} (TOC_{SCS}(1 - R_{Kuroshio}) + TOC_{Kuroshio} R_{Kuroshio})}{500} \\ &= \frac{\sum_{Z=0}^{Z=500m} (TOC_{SCS} + (TOC_{Kuroshio} - TOC_{SCS}) R_{Kuroshio})}{500} \\ &= \frac{\sum_{Z=0}^{Z=500m} TOC_{SCS}}{500} \\ &\quad + \frac{\sum_{Z=0}^{Z=500m} (TOC_{Kuroshio} - TOC_{SCS}) R_{Kuroshio}}{500} \end{aligned} \quad (10)$$

where TOC_{Model} is the TOC concentration in each water layer of the upper 500 m layer in the outflow (eastward) or inflow (westward) water, predicted by the isopycnal mixing model; and TOC_{SCS} and

$TOC_{Kuroshio}$ are the TOC concentrations of the SCS and Kuroshio endmembers. $R_{Kuroshio}$ are the Kuroshio water fractions in the outflow or inflow water. $\frac{\sum_{Z=0}^{Z=500m} TOC_{SCS}}{500}$ is the depth-averaged TOC concentration of the SCS water proper, and $\frac{\sum_{Z=0}^{Z=500m}(TOC_{Kuroshio}-TOC_{SCS})R_{Kuroshio}}{500}$ is the depth-averaged TOC concentration of the excess TOC contributed by the Kuroshio water, which was denoted as $C_{Kuroshio-TOC}$. Since TOC concentrations of the SCS water proper (TOC_{SCS}) are known, Eq. (10) could be simplified as

$$C_{depth-averaged} = (52.1 \pm 0.6) + C_{Kuroshio-TOC} \quad (11)$$

Substituting this $C_{depth-averaged}$ into Eq. (9), we get

$$\begin{aligned} F_{Net} &= F_{Outflow} - F_{Inflow} \\ &= f_{Eastward}C_{Eastward} - f_{Westward}C_{Westward} \\ &= (52.1 \pm 0.6)(f_{Eastward} - f_{Westward}) \\ &\quad + f_{Eastward}C_{Kuroshio-TOC-Eastward} \\ &\quad - f_{Westward}C_{Kuroshio-TOC-Westward} \\ &= (52.1 \pm 0.6)f_{Net} + f_{Eastward}C_{Kuroshio-TOC-Eastward} \\ &\quad - f_{Westward}C_{Kuroshio-TOC-Westward} \end{aligned} \quad (12)$$

where $f_{Eastward}$, $f_{Westward}$ and f_{Net} are eastward, westward and net water flow flux in the upper layer; and $C_{Kuroshio-TOC-Eastward}$ and $C_{Kuroshio-TOC-Westward}$ are the depth-averaged TOC concentrations of excess TOC contributed by Kuroshio water in the eastward and westward flow water.

Thus, the net transport flux of TOC in the upper layer was composed of both $(52.1 \pm 0.6)f_{Net}$, which denotes the net TOC exchange flux due to the net water exchange, and $f_{Eastward}C_{Kuroshio-TOC-Eastward} - f_{Westward}C_{Kuroshio-TOC-Westward}$, which denotes the net transport flux of excess TOC, due to the TOC concentration gradient in the upper layer.

The uncertainty of F_{Net} is mostly dependent on the uncertainties in f_{Net}, $f_{Eastward}$, $f_{Westward}$, $C_{Kuroshio-TOC-Eastward}$ and $C_{Kuroshio-TOC-Westward}$. Based on the water fluxes reported (Liao et al., 2008; Yang et al., 2010, 2011; Hsin et al., 2012; Xu and Oey, 2014), we obtained that f_{Net}, $f_{Eastward}$ and $f_{Westward}$ were -5.2 ± 2.8, 4.1 ± 4.3 and -4.3 ± 6.1 Sv. The uncertainties of $C_{Kuroshio-TOC-Eastward}$ and $C_{Kuroshio-TOC-Westward}$ are dependent on the uncertainties of TOC concentrations of the SCS and Kuroshio water endmembers, $R_{Kuroshio-Eastward}$ and $R_{Kuroshio-Westward}$. Based on the T–S distributions in the Luzon Strait, which were shown in the published papers reporting the $f_{Westward}$ and $f_{Eastward}$, we estimated that the uncertainties of $R_{Kuroshio-Eastward}$ and $R_{Kuroshio-Westward}$ were 0.13 and 0.22 using the isopycnal mixing model. Thus, we calculated that the F_{Net} in the upper layer was -107.1 ± 54.6 Tg C yr^{-1}. Among which, 97% was contributed by the fraction of $(52.1 \pm 0.6)f_{Net}$, suggesting that the net TOC transport induced by the net water exchange was dominant. Note that the residual 3% of the net TOC transport (3.2 ± 1.6 Tg C yr^{-1}) induced by the TOC concentration gradient was approximately identical to the increase in the area-integrated TOC inventory (3.5 Tg) in the NSCS owing to the Kuroshio intrusion (in Section 4.1), proving that our estimation was in order.

4.3.2. Net TOC transport flux through the Luzon Strait in the intermediate and deep layers

Although we observed that the TOC concentration at 1000–1500 m in the SCS basin was higher than that in the WPS (the difference was 2.6 ± 1.0) the depth-averaged TOC concentration in the intermediate layer (500–1500 m) along the section at 120°E was relatively constant at 43.6 ± 1.2 μmol L^{-1}, which was also confirmed by the isopycnal mixing model. Here, because $C_{Westward} \approx C_{Eastward}$, Eq. (9) could be simplified as

$$\begin{aligned} F_{Net} &= F_{Outflow} - F_{Inflow} \\ &= f_{Eastward}C_{Eastward} - f_{Westward}C_{Westward} \\ &= (f_{Eastward} - f_{Westward})C_{Westward} \\ &= f_{Net}C_{Westward} \end{aligned} \quad (13)$$

Based on the f_{Net} values reported in Hsin et al. (2012) and Xu and Oey (2014) we calculated a net export flux of TOC, ranging from 78.5 to 218 Tg C yr^{-1}, with an average of 54.7 ± 15.0 Tg C yr^{-1}.

Similar for the intermediate layer transport, the deep layer inflow flux of TOC from the WPS could also be estimated using Eq. (13). Here, the water flux was relatively constant, ranging from -0.1 to -2.0 Sv (Xu and Oey, 2014 and references therein). The uncertainty of the inflow flux was probably related to the seasonal variations of the volume transport, due to the seasonal variability in water properties of the Pacific (Zhao et al., 2014). Because TOC concentration of the deep water in the SCS was the same as in the WPS, the net TOC transport flux in the deep layer was controlled by the net water flux, and calculated by multiplying net water flux by TOC concentration in the deep water (40 μmol L^{-1}). We calculated a net input flux of TOC, ranging from -1.5 to -30.3 Tg C yr^{-1}, with an average of -16.4 ± 13.1 Tg C yr^{-1}.

Integrating the three-layers, the total net exchange flux of TOC through the Luzon Strait was -68.8 ± 58.0 Tg C yr^{-1}, indicating that the inflow of organic material to the SCS through the Luzon Strait was considerably higher than the outflow, and that the SCS acted as a sink of organic carbon for the WPS.

We must point out that the above estimate of TOC exchange fluxes was subject to considerable uncertainty. Among other things, the largest variability was mainly due to the great uncertainty of water exchange flux in the upper layer. This was because the Kuroshio intrusion in the upper layer contributes most to the Luzon Strait transport (Nan et al., 2014 and references therein), and the water flux displayed highly seasonal variations, ranging from -0.8 to -10.3 Sv. Thus, in order to reduce the uncertainty of the TOC exchange flux, more long-term consecutive observations or modeling studies are needed to constrain the water flux. In addition, the seasonal variations of TOC concentration in the Kuroshio water might also bring uncertainties.

Despite the relatively large uncertainty, the exchange of TOC between the SCS and WPS has important implications. Concerning the export of TOC in the intermediate layer, Dai et al. (2009) suggest that the excess TOC is likely to be from the freshly fixed organic carbon in the upper SCS, and this will contribute significantly to carbon sequestration. On the other hand, the inflow TOC, which was accumulated in the upper layer of the WPS owing to the low nutrient levels suppressing the bacterial uptake of DOM (Shiah et al., 1998) could be respired in the SCS, under the conditions of the higher nutrient levels supplied in the SCS (Du et al., 2013). At the same time, the respiration of the inflow TOC might have contributed to the inventory of inorganic nutrients in the upper layer of the SCS.

5. Concluding remarks

Both TOC concentrations and their inventory in the upper 100 m of the central NSCS displayed significant spatial variations. The TOC concentration and inventories were overall higher in the east relative to the west of the central NSCS. This was consistent with the Kuroshio water fraction distribution in the NSCS. The TOC inventories in the upper 100 m were relatively high in fall but low in spring and winter. In addition to the mesoscale eddy and upwelling, the Kuroshio intrusion played a dominant role in

determining the TOC inventory distribution in the central NSCS. As well as the Kuroshio intrusion in the upper layer, we observed net TOC production in the upper 100 m during fall and winter. In the intermediate layer water, there existed a net outflow flux of TOC from the SCS, amounting to 54.7 ± 15.0 Tg C yr^{-1}. In both the upper and deeper layers, there were influxes of TOC from the WPS to the SCS. The net exchange flux of TOC through the entire Luzon Strait was -68.8 ± 58.0 Tg C yr^{-1}. We noted that the exchange of TOC between the SCS and WPS has important implications in terms of production, and the bioavailability and fate of dissolved organic carbon, both for the SCS and WPS as well as the Pacific Ocean at large.

Acknowledgments

This work was funded by the National Basic Research Program (973) sponsored by the Ministry of Science and Technology through Grant 2015CB954001, and the National Natural Science Foundation of China through Grants 91328202, 41121091, 90711005 and 41130857. We are grateful to the captain and crew members on R/V Dongfanghong as well as Pinghe Cai and Weidong Zhai for their help during the cruises. Professor John Hodgkiss is thanked for his help with English.

References

Biscaye, P.E., Flagg, C.N., Falkowski, P.G., 1994. The shelf edge exchange processes experiment, SEEP-II: an introduction to hypotheses, results and conclusions. Deep-Sea Res. II 41, 231–252.

Broecker, W.S., Patzert, W.C., Toggweiler, J.R., Stuiver, M., 1986. Hydrography, chemistry, and radioisotopes in the Southeast Asian basins. J. Geophys. Res. 91, 14345–14354. http://dx.doi.org/10.1029/JC091iC12p14345.

Chao, S.Y., Shaw, P.T., Wu, S.Y., 1996. El Niño modulation of the South China Sea circulation. Prog. Oceanogr. 38, 51–93.

Cai, P.H., Zhao, D.C., Wang, L., Huang, B.Q., Dai, M.H., 2015. Role of particle stock and phytoplankton community structure in regulating particulate organic carbon export in a large marginal sea. J. Geophys. Res. Oceans 120, 2063–2095. http://dx.doi.org/10.1002/2014JC010432.

Chen, C.T.A., Wang, S.L., Wang, B.J., 2001. Nutrient budgets for the South China Sea basin. Mar. Chem. 75, 281–300.

Chen, Y.L., Chen, H.Y., 2006. Seasonal dynamics of primary and new production in the northern South China Sea: the significance of river discharge and nutrient advection. Deep-Sea Res. I 53, 971–986.

Chen, B.Z., Liu, H.B., Huang, B.Q., 2012. Environmental controlling mechanisms on bacterial abundance in the South China Sea inferred from generalized additive models (GAMs). J. Sea Res. 72, 69–76.

Chu, P.C., Li, R.F., 2000. South China Sea isopycnal-surface circulation. J. Phys. Oceanogr. 30, 2419–2438.

Civitarese, G., Gacic, M., Vetrano, A., Boldrin, A., Bregant, D., Rabitti, S., Souvermezoglou, E., 1998. Biogeochemical fluxes through the Strait of Otranto (Eastern Mediterranean). Cont. Shelf Res. 18, 773–789.

Dai, M.H., Meng, F.F., Tang, T.T., Kao, S.J., Lin, J.R., Chen, J.H., Huang, J.C., Tian, J.W., Gan, J.P., Yang, S., 2009. Excess total organic carbon in the intermediate water of the South China Sea and its export to the North Pacific. Geochem. Geophys. Geosyst. 10, Q12002. http://dx.doi.org/10.1029/2009GC002752.

Dai, M.H., Cao, Z., Guo, X., Zhai, W., Liu, Z., Yin, Z., Xu, Y., Gan, J., Hu, J., Du, C., 2013. Why are some marginal seas sources of atmospheric CO_2? Geophys. Res. Lett. 40, 2154–2158. http://dx.doi.org/10.1002/grl.50390.

Du, C.J., Liu, Z.Y., Dai, M.H., Kao, S.J., Cao, Z.M., Zhang, Y., Huang, T., Wang, L.F., Li, Y., 2013. Impact of the Kuroshio intrusion on the nutrient inventory in the upper northern South China Sea: insights from an isopycnal mixing model. Biogeoscience 10, 6419–6432.

Gan, J., Li, H., Curchitser, E.N., Haidvogel, D.B., 2006. Modeling South China Sea circulation: response to seasonal forcing regimes. J. Geophys. Res. 111, C06034. http://dx.doi.org/10.1029/2005JC003298.

Gomez, F., 2003. The role of the exchanges through the Strait of Gibraltar on the budget of elements in the Western Mediterranean Sea: consequences of human-induced modifications. Mar. Pollut. Bull. 46, 685–694.

Hansell, D.A., Carlson, C.A., 1998. Net community production of dissolved organic carbon. Glob. Biogeochem. Cycles 12, 443–453.

Hsin, Y.C., Wu, C.R., Chao, S.Y., 2012. An updated examination of the Luzon Strait transport. J. Geophys. Res. 117, C03022. http://dx.doi.org/10.1029/2011JC007714.

Huthnance, J.M., Holt, J.T., Wakelin, J.T., 2009. Deep ocean exchange with West-European shelf seas. Ocean Sci. 5, 621–634.

Jahnke, R.A., Roman, M.R., Brink, K.H., 2008. Coastal ocean processes program: advancing interdisciplinary research and technology development. Oceanography 21, 18–21.

Krom, M.D., Herut, B., Mantoura, R.F.C., 2004. Nutrient budget for the Eastern Mediterranean: implications for phosphorus limitation. Limnol. Oceanogr. 49 (5), 1582–1592.

Li, L., Qu, T., 2006. Thermohaline circulation in the deep South China Sea basin as inferred from oxygen distributions. J. Geophys. Res. 111, C05017. http://dx.doi.org/10.1029/2005JC003164.

Lin, I.I., Chen, J.P., Wong, G.T.F., Huang, C.W., Lien, C.C., 2007. Aerosol input to the South China Sea: results from the moderate resolution imaging spectro-radiometer, the quick scatterometer and the measurements of pollution in the troposphere sensor. Deep-Sea Res. II 54, 1589–1601.

Liu, K.K., Chao, S.Y., Shaw, P.T., Gong, G.C., Chen, C.C., Tang, T.Y., 2002. Monsoon-forced chlorophyll distribution and primary production in the South China Sea: observations and a numerical study. Deep-Sea Res. I 49, 1387–1412.

Liu, K.K., Wang, L.W., Dai, M., Tseng, C.M., Yang, Y., Sui, C.H., Oey, L., Tseng, K.Y., Huang, S.M., 2013. Inter-annual variation of chlorophyll in the northern South China Sea observed at the SEATS Station and its asymmetric responses to climate oscillation. Biogeoscience 10, 7449–7462.

Liao, G.H., Yuan, Y.C., Xu, X.H., 2008. Three dimensional diagnostic study of the circulation in the South China Sea during winter 1998. J. Oceanogr. 64, 803–814.

Nan, F., Xue, H.J., Yu, F., 2014. Kuroshio intrusion into the South China Sea: A review. Prog. Oceanogr. http://dx.doi.org/10.1016/j.pocean.2014.05.012, in press.

Qu, T., Mitsudera, H., Yamagata, T., 2000. Intrusion of the North Pacific waters into the South China Sea. J. Geophys. Res. 105, 6415–6424.

Qu, T.D., Girton, J.B., Whitehead, J.A., 2006. Deep water over flow through Luzon Strait. J. Geophys. Res. 111, C01002. http://dx.doi.org/10.1029/2005JC003139.

Siegenthaler, U., Sarmiento, J.L., 1993. Atmospheric carbon dioxide and the ocean. Nature 365, 119–125.

Shaw, P.T., 1991. The seasonal variation of the intrusion of the Philippine Sea water into the South China Sea. J. Geophys. Res. 96, 821–827.

Shaw, P.T., Chao, S.Y., 1994. Surface circulation in the South China Sea. Deep-Sea Res. I 41, 1663–1683.

Shiah, F.K., Kao, S.J., Liu, K.K., 1998. Bacterial production in the western equatorial Pacific: implications of inorganic nutrient effects on dissolved organic carbon accumulation and consumption. Bull. Mar. Sci. 63, 795–808.

Tian, J.W., Yang, Q.X., Liang, X.F., Xie, L.L., Hu, D.X., Wang, F., Qu, T.D., 2006. Observation of Luzon Strait transport. Geophys. Res. Lett. 33, L19607. http://dx.doi.org/10.1029/2006GL026272.

Xu, F.H., Oey, L.Y., 2014. State analysis using the Local Ensemble Transform Kalman Filter (LETKF) and the three-layer circulation structure of the Luzon Strait and the South China Sea. Ocean Dyn. 64, 905–923.

Yang, Q., Tian, J., Zhao, W., 2010. Observation of Luzon Strait transport in summer 2007. Deep-Sea Res. I 57, 670–676.

Yang, Q.X., Tian, J.W., Zhao., W., 2011. Observation of material fluxes through the Luzon Strait. Chin. J. Oceanol. Limnol. 29 (1), 26–32.

Yuan, Y.C., Liao, G.H., Guan, W.B., Wang, H.Q., Lou, R.Y., Chen, H., 2008. The circulation in the upper and middle layers of the Luzon Strait during spring 2002. J. Geophys. Res. Oceans 113, C06004. http://dx.doi.org/10.1029/2007JC004546.

Zhao, W., Zhou, C., Tian, J., Yang, Q., Wang, B., Xie, L., Qu, T., 2014. Deep water circulation in the Luzon Strait. J. Geophys. Res. Oceans 119, 790–804. http://dx.doi.org/10.1002/2013JC009587.